

This is the final draft of the contribution published as:

May, J.C., Jurneczko, E., Stow, S.M., **Kratochvil, I., Kalkhof, S.**, McLean, J.A. (2018):
Conformational landscapes of ubiquitin, cytochrome c, and myoglobin: Uniform field ion
mobility measurements in helium and nitrogen drift gas
Int. J. Mass Spectrom. **427** , 79 - 90

The publisher's version is available at:

<http://dx.doi.org/10.1016/j.ijms.2017.09.014>



Published in final edited form as:

Int J Mass Spectrom. 2018 April ; 427: 79–90. doi:10.1016/j.ijms.2017.09.014.

Conformational Landscapes of Ubiquitin, Cytochrome c, and Myoglobin: Uniform Field Ion Mobility Measurements in Helium and Nitrogen Drift Gas

Jody C. May^a, Ewa Jurnecko^a, Sarah M. Stow^{a,1}, Isabel Kratochvil^{b,2}, Stefan Kalkhof^{c,3}, and John A. McLean^a

^aDepartment of Chemistry, Center for Innovative Technology, Vanderbilt Institute for Integrative Biosystems Research and Education, and Vanderbilt Institute of Chemical Biology, Vanderbilt University, Nashville, Tennessee, 37235, United States

^bInstitute of Biochemistry, Faculty of Biosciences, Pharmacy and Psychology, Leipzig University, 04103 Leipzig, Germany

^cDepartment of Molecular Systems Biology, Helmholtz-Centre for Environmental Research - UFZ, 04318 Leipzig, Germany

Abstract

In this study, a commercial uniform field drift tube ion mobility-mass spectrometer (IM-MS) was utilized to measure the gas-phase conformational populations of three well-studied proteins: ubiquitin (8566 Da), cytochrome c (12,359 Da), and myoglobin in both apo and holo forms (16,951 and 17,567 Da, respectively) in order to evaluate the use of this technology for broadscale structural proteomics applications. Proteins were electrosprayed from either acidic organic (pH ~3) or aqueous buffered (pH ~6.6) solution phase conditions, which generated a wide range of cation charge states corresponding to both extended (unfolded) and compact (folded) gas-phase conformational populations. Corresponding collision cross section (CCS) measurements were compiled for significant ion mobility peak features observed at each charge state in order to map the conformational landscapes of these proteins in both helium and nitrogen drift gases. It was observed that the conformational landscapes were similar in both drift gases, with differences being attributed primarily to ion heating during helium operation due to the necessity of operating the instrument with higher pressure differentials. Higher resolving powers were observed in nitrogen, which allowed for slightly better structural resolution of closely-spaced conformer populations. The instrumentation was found to be particularly adept at measuring low abundance conformers which are only present under gentle conditions which minimize ion heating. This work

Corresponding Author: John A. McLean, VU Station B #351822, 2301 Vanderbilt Place, Nashville, TN 37235-1822, john.a.mclean@vanderbilt.edu.

¹Present Address: Agilent Technologies, Santa Clara, CA, USA

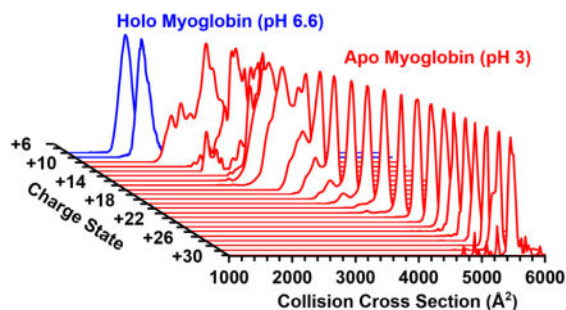
²Present Address: Department of Molecular Systems Biology, Helmholtz-Centre for Environmental Research - UFZ, Permoserstraße 15, 04318 Leipzig, Germany

³Present Address: Institute of Bioanalysis, University of Applied Sciences and Arts of Coburg, 96450 Coburg, Germany

Publisher's Disclaimer: This is a PDF file of an unedited manuscript that has been accepted for publication. As a service to our customers we are providing this early version of the manuscript. The manuscript will undergo copyediting, typesetting, and review of the resulting proof before it is published in its final citable form. Please note that during the production process errors may be discovered which could affect the content, and all legal disclaimers that apply to the journal pertain.

represents the single largest ion mobility CCS survey published to date for these three proteins with 266 CCS values and 117 ion mobility spectra, many of which have not been previously reported.

Graphical abstract



1. Introduction

The proteins cytochrome c, ubiquitin, and myoglobin are among the three most studied analytes in ion mobility-mass spectrometry (IM-MS) research with over one thousand collision cross section (CCS) measurements published for these three proteins. The large number of reported CCS values is attributed in part to the high degree of structural heterogeneity exhibited by proteins, but is also a result of unique CCS values populated by each of the numerous charge states formed during the electrospray process as well as the necessity to report gas-specific CCS measurements, such as those obtained in nitrogen and helium drift gases. Additionally, these proteins are considered model systems by the IM and MS communities, and as such the reporting of CCS measurements serves as a form of validation for new IM techniques and approaches.[1] Despite their use as analytical standards, there is a great deal of ion mobility information which is still unavailable, such as conformer populations for specific charge state and the relative populations of conformers across different drift gases.

Ubiquitin, cytochrome c, and myoglobin were extensively studied by ion mobility in the 1990s during a period of foundational activity in biological IM-MS, initiated in response to the development of ESI and MALDI techniques. Electrosprayed cytochrome c was the first protein IM spectrum published. The spectrum was obtained by Richard Smith and coworkers at Pacific Northwest National Laboratory (PNNL) using a drift tube operated at ambient pressure.[2] Higher resolution IM measurements of cytochrome c were later described by Herbert Hill and coworkers and demonstrated charge state separation for ESI generated protein ions.[3, 4] The CCS of ubiquitin, cytochrome c, and myoglobin were initially determined by Douglas and coworkers using an energy loss technique implemented in a triple quadrupole MS, which indicated that protein CCS values depended on the nature of the solvent system used (i.e., aqueous or organic).[5] A few years later, Clemmer, Jarrold and coworkers described the first of a series of extensive CCS surveys of protein charge states and conformations for these three proteins.[6–9] In these studies, CCS values were measured using a drift tube operated in helium drift gas ($^{DT}CCS_{He}$). These first IM-MS

measurements are considered seminal contributions to the field of quantitative ion mobility research, and CCS values for these proteins are routinely used for calibration and validation of ion mobility instrumentation and related techniques.[10–15]

Ubiquitin, cytochrome c, and myoglobin exhibit similar behavior in the IM-MS experiment: higher charge states present themselves as a single or narrow distribution of conformers, whereas intermediate charge states populate a wide range of conformers that span a large CCS range. The relative populations of conformers observed at these intermediate charge states are highly sensitive to experimental conditions such as solution phase pH, ion source temperatures and voltages, as well as gas-phase ion heating.[7, 8, 16, 17] At low charge states, these proteins exhibit a narrow set of conformers which lie in the range of theoretically predicted CCS values obtained from X-ray crystal structures. It is also unclear whether the drift gas composition directly affects the conformational landscapes sampled by the IM-MS experiment, as previous work has suggested.[18]

In this study, the three proteins, ubiquitin, cytochrome c, and myoglobin, are analyzed using contemporary drift tube IM-MS. This study serves three primary purposes: (1) to evaluate the use of a commercial drift tube instrument for structural proteomics applications, (2) to bring together ion mobility findings for different charge states and drift gases into a single body of work, and (3) to confirm previous observations regarding the conformational populations of these proteins. The instrument used here is a commercial IM-MS developed by Agilent Technologies which is based on extensive IM-MS research from Richard Smith and coworkers at PNNL. This instrument is based on a PNNL IM-MS design[19, 20] which utilizes electrodynamic ion funnels for focusing ions both before and after the drift tube,[12, 21, 22] as well as an “hourglass” ion funnel trap[23] for storing and modulating ion pulses into the uniform field drift region.[24] Noteworthy is that the three proteins evaluated in this study were initially utilized by Smith and coworkers to characterize the first electrodynamic ion funnel described in the literature.[25] In addition to the extensive use of ion funnel technology, the instrument also supports temporal multiplexing based on pseudorandom sequences,[26, 27] and 4-dimensional feature finding algorithms for mining LC-IM-MS data,[28] which are all based on technologies developed at PNNL.

2. Materials and Methods

2.1. Sample Preparation

Protein standards: ubiquitin from bovine erythrocytes, cytochrome c and myoglobin from equine heart were obtained as lyophilized powders (Sigma Aldrich). All standards were reconstituted as received in high purity water and stored at *ca.* -4 °C before further dilution. Initial stock solutions of 1 mg/ml of all proteins were prepared in 18 MΩ deionized water (Milli-Q, Millipore). Myoglobin sample was in addition dialyzed overnight (Slider-A-Lyzer Dialysis Cassettes) to remove excess salts. Two sets of analytical stock solutions at *ca.* 1 ug/mL were prepared in aqueous buffered (high pH) and organic acidified (low pH) solution conditions. All buffered samples were prepared in 20 mM ammonium acetate (77.08 g/mol, 99% purity, Fisher Scientific), whereas samples in the organic solvents were prepared in 50 % methanol/50 % water with 0.2 % formic acid. High purity water, methanol (optima LC-MS grade, Fisher Scientific) and formic acid (99% purity, VMD International Ltd.)

were used as received from the vendors. The pH of each prepared sample solution was measured using a pH meter (SevenEasy, Mettler-Toledo, Columbus, OH), and corresponded to a pH range between 2.7 and 3.8 for acidic organic samples and a pH range between 6.5 and 6.7 for aqueous buffered samples. The pH values were measured after all experiments to minimize contamination due to sample carryover.

2.2 Instrumentation and Experimental Parameters

The instrument utilized in this work is a commercial IM-MS instrument based on a drift tube ion mobility spectrometer interfaced to a time-of-flight mass spectrometer (Ion Mobility Q-TOF MS 6560, Agilent Technologies, Santa Clara, CA).[29, 30] A schematic of the Agilent IM-MS platform is contained in Figure 1. Ions were produced by positive mode nano-electrospray ionisation (nESI, G1992A Nanospray, Agilent) configured in the orthogonal orientation (Figure 1A). Borosilicate glass emitters were prepared in-house for nESI using a laser-based micropipette puller (Model P-2000, Sutter Instrument Company, Novato, CA, USA) and then filled with *ca.* 10 μ L of sample solution by means of gel micro-loading tips (Eppendorf, Hamburg, Germany). Following nESI, ions are directed orthogonally by a counter electrode into a resistively coated single-bore glass capillary. The glass capillary entrance defines the nESI spray field which allows for the glass emitter to be operated at ground potential, while the exit end of the ion transfer capillary within the vacuum system (Figure 1B) can be biased as high as *ca.* 2100 V. This facilitates high voltage operation of the drift tube. The distance of the sample emitter from the counter electrode and the spray shield was adjusted to provide an optimum spray, as determined by the spray stability and maximum ion counts. The ion source drying gas was nitrogen operated at a flow rate of 13 L/min at ambient temperature (25 °C) to minimize unfolding effects, as previously noted. [16] Ions exiting the resistive capillary are transferred through ion optics into a tandem ion funnel interface incorporating a high-pressure (4.3 to 4.8 Torr) transmission ion funnel (Figure 1C) followed by a trapping ion funnel (Figure 1D) which incorporates a dual-grid ion gate. Briefly, the trapping ion funnel allows for the accumulation and modulation of ions into temporally narrow ion packets which are gated into the drift tube. Experimental parameters for the tandem ion funnel configuration were as follows: high-pressure funnel radio-frequency (RF) of 80 Vpp (peak-to-peak) at 1.5MHz, and 150 V DC, trapping funnel RF of 80 Vpp at 1.2 MHz, 120 V DC. The drift tube (Figure 1E) is a uniform field DC-only design of 78.24 cm total length.[31] The drift tube was operated at ambient (*ca.* 298 K) temperature, while the pressure of IM drift gas (high purity helium or nitrogen, UHP 5.0 grade) was maintained at 3.95 Torr using a vendor-supplied gas control kit (alternate gas kit, Agilent) which consists of a gas flow controller (Figure 1F) monitoring an absolute pressure transducer (CDG-500, Agilent). Upon exiting the drift region, ions are refocused axially by means of a rear ion funnel (Figure 1G) operated with an RF of 80 Vpp at 1.2 MHz and a 100 V DC. Ions exit the rear funnel into a differential pressure interface region where they are transferred via a resistively coated hexapole ion guide (Figure 1H). Following the hexapole, ions are introduced into a modified quadrupole time-of-flight mass spectrometer (Q-TOFMS), which consists of a quadrupole mass analyser (Figure 1I), a hexapole collision cell (Figure 1J), and a beam compressor with combined shaping and steering optics (Figure 1K), prior to reaching the TOF analyser (Figure 1L–N). MassHunter software was utilized for all data acquisition (IM-MS Data Acquisition) and 2D IM-MS data processing (IMS Browser).

CCS measurements were obtained within a mass window between m/z 50 and 3200, although the instrument was also tuned to high mass transmission mode (m/z 10,000) in order to evaluate the presence of multimers and low charge state analytes, which were not observed under these experimental conditions. Multimers were observed at higher sample concentration (~ 100 $\mu\text{g/mL}$) which appear within the m/z ranges of the monomers, however, these signals were far removed from the primary ATDs of the monomer, and so could be accounted for. Specifically, at high sample concentrations, multimer ATDs appear at lower and higher drift times from the monomer ATDs due to post-mobility dissociation of singly-charged, and multiply-charged aggregates, respectively.

2.3 Experimental Conditions for Alternative Drift Gases

An extensive screening of experimental parameters (voltages and pressures) was performed to attain an optimal signal (highest resolution of conformers) and good ^{DT}CCS measurement reproducibility in each of the drift gases utilized. The gas purity within the drift tube (especially when operating in helium) was ensured by careful optimization of the gas pressure difference between the tandem ion funnel interface and drift tube, which affects the degree of source gas intrusion (primarily nitrogen) into the IM stage as previously noted.[32, 33] Gas intrusion into the drift tube manifests as higher drift times for helium operation, which results in erroneously high $^{DT}CCS_{He}$ values. Specifically, the drift tube is operated at an elevated pressure with respect to the ion funnel trap region, with a pressure differential of greater than *ca.* 150 mTorr for nitrogen and 230 mTorr for helium. Because of different Paschen electrical discharge limits between nitrogen and helium, the drift potential was operated between 850 to 1450 V for nitrogen (E/N ratio of 9 to 15 Td), while for helium, a reduced voltage range of 650 to 1250 V was utilized (E/N ratio of 7 to 13 Td). For helium, it was found that dielectric voltage breakdown would occur at fields exceeding these values, which manifested as excessive spectral noise at the low m/z region of the IM-MS spectra.

An additional consideration when operating with helium drift gas is that lower resolving powers are accessible in contrast to nitrogen, and to achieve optimal helium resolving powers require smaller temporal ion gate widths. For example, in nitrogen, the highest IM resolving powers are obtained at a temporal gate width between 150 and 200 μs , whereas helium requires gate widths between 100 and 150 μs . This is a consequence of the higher mobility of ions in helium, and this observation has been previously discussed in detail.[30] In some cases, the gate width is increased to enhance sensitivity at a cost of resolving power, which allows CCS measurements for low abundance signals (e.g., low and high m/z ions) to be obtained, as well as to enhance the signal-to-noise for minor protein conformers. Finally, there is evidence of higher sensitivity in helium than nitrogen, which is attributed to increased helium gas intrusion into the ion funnel trap, allowing it to operate more efficiently, as previously noted.[34]

2.4. Optimization of Parameters to Produce Compact CCS Populations

A goal of native mass spectrometry is to preserve tertiary protein structure in order to probe complex topology and dynamics,[35] where the experimental parameters are selected systematically to achieve optimum signal while avoiding any instrument-induced structural transitions. During preliminary experiments, it was observed that more gentle ion source and

ion transfer conditions resulted in a transition of low charge state IM populations to more compact CCS values, which is interpreted as the ions forming compact conformers in the gas-phase. Compact conformations were observed with the three ion funnels (high pressure, trapping, and rear) operating at a low RF amplitude of 80 Vpp. Below this value, ion transmission drops sharply and useful signal is difficult to obtain. As can be expected, the trapping ion funnel had the most drastic effect on protein conformational populations, and while the RF amplitude of the high pressure and rear ion funnels did not appear to affect the CCS values measured, these were nonetheless kept low (80 Vpp) to ensure that minimal ion heating was occurring. In addition to low RF values, the ionization source was operated at a low drying gas temperature of 25 °C, and the nESI emitter potential was operated in the range of 1000–1200 V. Under these conditions, sensitivity was low but suitable IM-MS spectra could still be obtained.

2.5. Collision Cross Section Measurements

For mostly or completely resolved IM peak features, the centroid drift time value obtained from IM-MS Browser (Agilent) is used for the CCS calculations. For partially-resolved features, drift times were manually extracted once these features were confirmed to be reproducible across all drift fields. We note that it is not always possible to obtain CCS values for partially-resolved features due to a previously-observed loss in fine structure resolution at the higher drift fields surveyed,[33] thus, the number of features observed in the drift profile data does not necessarily correspond to the number of CCS values reported. The experimental drift times obtained from the IM peak profiles are uncorrected as they represent both the time ions take to traverse the drift tube and the transit time of ions spent outside the drift region (the non-mobility flight time), the latter representing ion transit through the interfacing IM-MS ion optics and MS. The non-mobility time component is determined from a plot of measured drift times versus the inverse drift voltage, referred to as a stepped-field method,[31] where a linear fit to the data will specify the value of the non-mobility time (y -intercept). This non-mobility time is subtracted from the uncorrected drift time to provide the corrected ion mobility drift time. These calculations are performed in the vendor supplied software (IM-MS Browser, Agilent). Subsequently, the rotationally-averaged gas-phase CCS is determined using the fundamental low field ion mobility equation (Mason-Schamp relationship), where drift gas parameters are corrected to standard conditions of temperature (276.15 K) and pressure (760 Torr). Aside from different drift field ranges, the procedure for determining ^{DT}CCS for helium and nitrogen is the same.

2.6. Calculation of Theoretical Collision Cross Sections

X-ray crystallography structures were downloaded from the Protein Data Bank for ubiquitin (1UBQ), cytochrome c (1HRC), and myoglobin (1VXG), and hydrogen atoms were added to each structure using XLEaP in the AMBER Software Suite.[36] The projected superposition approximation (PSA) method developed by Bowers and coworkers [37–40] was utilized to determine the theoretical CCS of the proteins in both helium and nitrogen drift gas from their crystal structure coordinates.

3. Results

3.1. Mass Spectra

When sprayed under both organic (red) and aqueous buffered (blue) conditions, all three proteins (ubiquitin, cytochrome c, and myoglobin) exhibit a broad distribution of low m/z signals under acidic organic conditions, and a narrow distribution of high m/z peaks under buffered conditions (Figure 2). Under both sets of solution phase conditions, a continuous series of protein charge states (Z) is observed for ubiquitin ($3 \leq Z \leq 16$), cytochrome c ($4 \leq Z \leq 24$), and myoglobin ($6 \leq Z \leq 30$), which allows a broad range of CCS values to be mapped for each protein. The highest charge states were only observed under high sensitivity settings (see section 2.3). Myoglobin (Figure 2C) contains a noncovalently bound heme group (m/z 616) which is only retained under buffered conditions (the holo form).

3.2. Ion Mobility Distributions

The IM spectrum for each charge state was extracted and aligned to their corresponding measured CCS values using a “single-field” drift time-CCS relationship which has been described previously. [31, 32] This allows IM spectra to be compared in CCS space for important relationships which may otherwise not be observed when evaluating raw drift time distributions.[33] IM spectra for all observed charge states in both helium and nitrogen drift gas are included in supporting information for ubiquitin (Figure S1), cytochrome c (Figure S2), and myoglobin (Figure S3).

Figures 3, 5, and 7 contain the gas-specific IM spectra for selected charge states of ubiquitin, cytochrome c, and myoglobin, respectively. The dark traces correspond to acidic organic solvent conditions (pH ~3), and light traces correspond to IM spectra obtained from aqueous buffered conditions (pH ~6.6). For myoglobin (Figure 5), the light traces represent the holo form. These IM distributions are qualitatively reproducible under the same experimental conditions, however, it is noted that minor changes in the relative heights of different ion features are observed across different experimental acquisitions, which indicates that the relative populations of conformers are sensitive to small changes in experimental conditions, such as spray voltage and tip morphology, as well as gas pressures in the transfer optics.

3.3 Drift Tube CCS Measurements

$DTCCS$ results from this study and from the literature are summarized for ubiquitin (Figure 4), cytochrome c (Figure 6), and myoglobin (Figure 8) for both helium and nitrogen drift gases. Error bars are included for the current CCS measurements (black filled circles) and represent the standard deviation obtained from replicate measurements. In most cases, the error bars are on the same size scale as the data points. While there have been numerous CCS measurements reported for these proteins from various IM techniques (e.g., TWIMS, TIMS, and FAIMS), only drift tube literature values are included in these analyses. A complete summary of CCS values obtained in this study and figures comparing these values to all known previously-published measurements are provided in the supporting information (Figures S4 to S6, Tables S1 to S4).

4. Discussion

The broad ranges of protein charge states observed in this work are noteworthy in that no specific strategies were used to generate low (e.g., charge reduction reactions, MALDI) or high (e.g., supercharging solvents) charge state populations. This observation is attributed to the high sensitivity ion funnels incorporated into the IM-MS utilized for these measurements. The ability to observe these low abundance charge states is particularly advantageous in that previous studies have demonstrated that gas-phase ion chemistry can have a significant effect on the conformer populations observed in ion mobility.[9, 41, 42]

4.1 Comparison of Helium and Nitrogen Conformational Space

In general, the IM spectra for the three proteins (Figures 3, 5 and 7) exhibit the same structural features in both helium and nitrogen drift gas. Similarities in the ion mobility distributions can be seen at the high and low charge states, where structural transitions are minimal. At the intermediate charge states where IM distributions differ, there are common features across both sets of gas-specific spectra. Nitrogen drift spectra are measured at a slightly higher resolving power than the helium spectra (*ca.* 60 versus 45, respectively, as determined from singly-charged calibrant ions), for reasons fundamental to the different mobilities in these gases.[30] This higher resolving power does not improve resolution of the broad IM distributions observed at intermediate and low charge states, but does result in better resolution of narrow CCS features at low and high charge states, notably ubiquitin +4, +10 and +11, cytochrome c +10, and myoglobin +7. This observation supports previous conclusions that the intermediate charge states for these proteins, where unfolding is observed, are comprised of numerous unresolved conformers. Descriptions of commonalities between spectra obtained in the different drift gases, as well as comparisons to the literature are discussed in the following sections for each protein.

4.2 Ubiquitin

From the body of IM-MS work published on the ubiquitin protein system, it is understood that this protein is characterized by three general structural regions in the gas-phase: a broad distribution of conformers at low CCS (compact region, or “C” state) which are stable under low energy conditions, an intermediate distribution (partially folded, or “P” state) which appears under moderate ion activation conditions, and a series of high CCS peaks (unfolded, or “U” state) which are sharp and appear as a result of the protein unfolding.[9, 17, 43, 44] In this study, a balance of experimental conditions was selected, which allows partially-folded conformers to be observed while retaining the sensitivity of the instrument to observe low abundance signals. Bowers and coworkers have shown that in a drift tube instrument configured similar to the one used in this work (i.e., nESI with ion funnel transfer to a drift tube), the folded conformers of ubiquitin can be observed at high abundance relative to the other conformers if special care is taken to impart minimal energy to the ions.[43] In this current study, only ubiquitin +7 measured in nitrogen demonstrates the simultaneous population of all three structural regions, and here these features are only partially-resolved, presumably due to an ensemble of unresolved conformers existing at the intermediate CCS values. In general, for each charge state it appears that more folded conformers are observed in nitrogen than in helium, which would suggest that more ion heating is occurring under the

conditions in which helium operates. This is likely due to the lower pressure operation of the ion trap needed to ensure gas purity in helium, which leads to a higher ion energy (higher E/N) prior to the drift tube. Overall, specific IM distributions observed here are consistent with the findings reported in the literature, with mostly folded conformers observed at low charge states (+4 to +6), broad distributions at intermediate charge states (+7 to +9), and narrow distributions of conformers again at high charge states (+10 and up). Charge states +10 to +12 are bimodal or have partial shoulder features. Ubiquitin +5 was reported in one previous account as bimodal by Clemmer and coworkers,[45] which correlates to the partial tail observed in this work. No direct electrospray observations have been previously published for ubiquitin +4 or +3, presumably due to the challenges associated with observing these charge states at high abundance. Ubiquitin +4 has been shown to exist as a single distribution when formed using charge-reduction ion chemistry,[9, 46] whereas at least two conformer populations are observed here. A bimodal distribution for ubiquitin +3 is also observed (Figure S1), which has not been previously reported.

Figure 4 compares all of the ubiquitin CCS values obtained in this present study (N=55, Table S1) with drift tube measurements published in the literature for helium and nitrogen (N=207).[9, 16, 45–53] An extended comparison which includes CCS measurements from other IM techniques (e.g., TWIMS, TIMS, FAIMS) is included as a supplemental figure (Figure S4). This current study includes the first $^{DT}CCS_{N_2}$ values reported for ubiquitin +3, +4, +15, and +16. The majority (79%) of ^{DT}CCS measurements have been obtained in helium drift gas.[54] In general, the CCS values obtained here correlate well with other measurements. For example, over 50 individual CCS values have been reported each for ubiquitin +11 and +10 (histograms, Figure 4C), and values obtained in this study fall near the center of the distribution of these measurements (black bars, Figure 4C). The scatter of data in both Figure 4A, 4B, and S4 demonstrate that similar conformational landscapes are sampled in all studies. For helium, there is a slight bias of current measurements to high CCS for the intermediate charge states (ubiquitin +7 and +8), which suggests the helium conditions used in this work may be contributing to some amount of protein unfolding. In contrast, the nitrogen measurements (Figure 4B) are highly consistent with published data.

The horizontal lines in Figures 4A and 4B correspond to the theoretical CCS values obtained from the X-ray crystal structure. A charge-state specific comparison is provided in Table S4. As has been previously demonstrated for proteins, the gas-phase CCS values of the lower charge states tend to be more compact than what is predicted from the crystal structure.[55] This observation is consistent in both drift gases.

4.3 Cytochrome C

Prior work has indicated that cytochrome c exhibits similar charge-state specific unfolding behaviour as ubiquitin when electrosprayed, with unfolding corresponding to a transition from low to high CCS, although the number of structural populations observed by IM-MS for cytochrome c appears to be higher.[6, 7, 56] Here, a broad range of conformers is observed for the majority of cytochrome c charge states (Figure 5), consistent with previous findings. As with ubiquitin, the unfolded conformers at high CCS are characterized with narrow distributions, which are predominant at the higher charge states starting with

cytochrome c +12. The unfolded features at high CCS are bimodal in most of the spectra. There is also a large number of folded and partially-folded features observed for cytochrome c +9 to +16 which have not been extensively reported in previous studies. It is unclear if this is due to the challenges associated with forming folded conformers for these higher charge states. In one exception, Barran and coworkers reported partially-folded conformers of cytochrome c +11, which could be unfolded to high CCS by operating a drift tube at temperatures in excess of 400K.[57] For the low charge states, cytochrome c +7 and +6 are observed as single distributions which are presumed to be mostly folded. Cytochrome c +6 in helium exhibits a bimodal distribution, whereas cytochrome c +5 (Figure S2) is bimodal when measured in both drift gases. The IM spectra for cytochrome c +4 was also obtained with poor signal-to-noise, but also appears to be bimodal in nitrogen drift gas, where resolving powers are higher (Figure S2). The differences in the spectra between helium and nitrogen are difficult to interpret. Unlike ubiquitin, more compact conformers appear in helium than nitrogen for cytochrome c, although it is unclear which gas-phase structures are more energetically stable as no energy-resolved IM spectra were obtained in this current study.

In Figure 6, the ^{DT}CCS values obtained in this work for cytochrome c (N=94, Table S2) are compared with values reported in the literature for helium (Figure 6A) and nitrogen (Figure 6B) drift gases (N=146).[7, 12, 48–51, 57–62] An extended literature comparison for cytochrome c is provided in Figure S5. Again, more ^{DT}CCS measurements (82%) have been made in helium than in nitrogen. In both drift gases, the higher CCS values for each charge state correlate well with values reported in the literature (c.f., Figure 6C), however significantly more low CCS features are observed in this study for cytochrome c +10 and higher. CCS values for cytochrome c +21 and higher have not been previously reported from drift tube measurements. Interestingly, for the higher charge states, cytochrome c exhibits the same decrease in CCS in response to charge as seen in ubiquitin, with a decrease in the CCS-to-charge slope observed in the plots in Figure 6.

The theoretical CCS values obtained from the cytochrome c x-ray crystal structure are projected as horizontal lines in Figure 6A and 6B. As with ubiquitin and other protein systems, the gas-phase CCS of lower charge states (here, cytochrome c +6 and +7) correlate the closest to the solution phase structure. The lowest charge states exhibit more compact structures than what the crystal structure predicts. Charge reduction studies from Badman and coworkers and MALDI measurements from Russell, McLean, and coworkers collectively demonstrate that cytochrome c +1 to +5 exhibit similar CCS values (Figure 6A). [50, 60, 61]

4.4 Myoglobin

The IM spectra and ^{DT}CCS values for myoglobin in its apo form was first described by Shelimov and Jarrold for the +4 to +20 cations, which demonstrated a broad unfolding transition between +6 and +10.[8, 56] More recent studies from Fernandez-Lima and coworkers noted multiple unfolded and partially folded conformers for apomyoglobin charge states from +9 to +13 and holomyoglobin +9, whereas a single distribution was observed for apomyoglobin +14 to +19 and holomyoglobin +8.[63, 64] In this present work,

myoglobin in its apo form was observed with multiple CCS features between +10 and +15 in both drift gases, similar to the observations from Fernandez-Lima and coworkers (Figure 7). The broad, asymmetric distributions observed for the intermediate charge states indicate that numerous conformers exist in these intermediate, partially folded regions of cross section space. In contrast, the higher charge states of apomyoglobin (+19 and up) are all characterized by a single, narrow peak, which suggests that the unfolded states of myoglobin exist as a narrow distribution of conformers. The low charge state measurements for holomyoglobin (+6 to +9) are characterized by a mostly folded distribution of conformers existing at low CCS. Holomyoglobin +7 is bimodal, and there is some evidence of at least two conformer populations also existing for holomyoglobin +6. These observations of multiple distributions at low charge state have not been previously reported for myoglobin. Regarding the differences observed in helium versus nitrogen, myoglobin exhibits complex behaviour. In most cases, lower CCS features are observed in helium, notably the +10, +11 and +13 charge states. This is more consistent with the results from cytochrome c, however, higher charge states (+15 to +20) demonstrate compact conformers (lower CCS features) in nitrogen. The original IM studies from Jarrold and coworkers indicated that myoglobin conformers have a preference for folding to lower CCS under high energy conditions,[8] which would support the observations made for ubiquitin that ion heating is occurring under helium conditions in this work.

A comparison of $DTCCS$ measurements for myoglobin from this study (N=117) and the literature (N=117) are contained in Figure 8 (and Figure S6 for other IM techniques) and demonstrate approximately the same conformational landscapes for the unfolded conformers at high charge states.[12, 18, 48, 50, 65] 71% of the literature CCS measurements for myoglobin were obtained in helium. Figure 6C contains the distribution analysis for two selected charge states of myoglobin (+13 and +14), however, the low numbers of reported $DTCCS_{He}$ values (N=9 and N=7, respectively) limit the information which can be derived from these projections. For the intermediate charge states where the unfolding transitions occur (myoglobin +7 to +12), previous CCS measurements in both helium and nitrogen are broadly distributed across a ca. 800 Å² range, with current measurements falling at the lower end of these values, indicating more compact conformers in these experiments. CCS values for apomyoglobin +27 to +31 (Table S3) have not been previously reported.. The observed differential increase in CCS with increasing number of charges gives rise to an “S” shaped conformational landscape for myoglobin, and this behavior is consistent with what is observed for ubiquitin and cytochrome c. A notable “dip” in the conformational landscape is observed at the higher charge states, particularly for the myoglobin +24 to +29 and the cytochrome c +19 to +23 regions. For all three proteins, the CCS change relative to charge state is approximately linear at the low and high charge state ranges, which is evidence of a gradual expansion of the gas-phase structure in response to increasing charge density. However, the abrupt change in CCS observed at the intermediate charge states is evidence that a Coulombic disruption of intermolecular forces is occurring in these protein systems.

Finally, the theoretical CCS value obtained from the X-ray crystal structure of myoglobin (horizontal line in Figure 8) lies along the same general region of the conformational landscape sampled in both drift gases, which correlates closest to the experimental CCS obtained for holomyoglobin +7, +8, and +9 (Table S4). This is consistent with previous

observations using theoretical CCS values obtained from the trajectory method which also used the X-ray crystal structure.[64]

5. Conclusions

The work presented here represents the most comprehensive survey of CCS measurements reported to date for the three well-studied proteins ubiquitin, cytochrome c, and myoglobin. Quantitative CCS findings are in general agreement with the body of work published on these proteins, which is remarkable given the high degree of structural heterogeneity that these proteins exhibit in the gas-phase. As noted by others, the specific conformer populations observed for each charge state are strongly dependent on the energy imparted on the ions prior to their measurement by ion mobility, and when care is taken to minimize ion heating, proteins tended to adopt compact CCS values. In general, the experimental parameters needed to operate with helium drift gas on this IM-MS platform (notably, high pressure differential prior to ion introduction into the drift tube) likely result in more ion heating due to a higher E/N value in the region, which manifests as more unfolded conformers observed for the intermediate protein charge states. While it is possible to operate the IM-MS instrumentation used in this work under conditions which minimize ion heating even further, such settings result in low instrument sensitivity and are generally not conducive to the type of comprehensive surveys focused on for this study. A report on more gentle instrument settings as well as an energy-resolved conformational survey of these proteins will be the subject of future studies. Specific solution-phase strategies to stabilize folded protein conformers may also help offset these instrumental ion heating effects.[66]

These broad and comprehensive studies are made possible by the advances in IM-MS instrumentation over the past few years. It is anticipated that the IM distributions (117 unique spectra) and corresponding CCS values (N=266) published in this current study will be useful for future researchers interested in using these proteins for their respective studies. In a more general sense, such data-intensive studies are critical for formulating generalized observations regarding the behaviour of anhydrous proteins as well as deriving practical information regarding the analytical measurements of such systems.

Supplementary Material

Refer to Web version on PubMed Central for supplementary material.

Acknowledgments

The authors gratefully acknowledge James N. Dodds and Katrina L. Leaprot for their assistance with acquiring data and preparing figures. This work was supported in part using the resources of the Center for Innovative Technology at Vanderbilt University. Funding for Vanderbilt authors was provided by the National Institutes of Health (NIH R01GM092218), the U.S. Army Research Office and the Defense Advanced Research Projects Agency (DARPA) under Cooperative Agreement Number W911 NF-14-2-0022, and the U.S. Environmental Protection Agency (EPA) under Assistance Agreement No. 83573601. Researchers from Helmholtz Centre for Environmental were supported by the Max Kade Foundation (IK) and the German Research Foundation DFG Transregio 67 subproject Z4 (SK). EJ and SMS also acknowledge a postdoctoral fellowship from Agilent Technologies. This work has not been formally reviewed by EPA and EPA does not endorse any products or commercial services mentioned in this publication. The views expressed in this document are solely those of the authors and should not be interpreted as representing the official policies, either expressed or implied, of the EPA, the Army Research Office, DARPA, or the U.S. Government.

Abbreviations

IM-MS	Ion Mobility-Mass Spectrometry
CCS	Collision Cross Section
^{DT}CCS	Drift Tube Collision Cross Section value
^{TW}CCS	Traveling Wave Collision Cross Section value
DC	Direct Current (i.e., Electrostatic)
E/N	Field-to-Number Density Ratio (in Townsend Units)
ESI	Electrospray Ionization
FAIMS	Field Asymmetric Ion Mobility Spectrometry
MALDI	Matrix Assisted Laser Desorption Ionization
PSA	Projected Superposition Approximation
RF	Radio Frequency (i.e., Electrodynamical)
TIMS	Trapped Ion Mobility Spectrometry
TWIMS	Traveling Wave Ion Mobility Spectrometry
V_{pp}	Peak-to-Peak Voltage
Z	Ion Integer Charge State

References

1. May JC, McLean JA. Ion Mobility-Mass Spectrometry: Time-Dispersive Instrumentation. *Anal Chem.* 2015; 87:1422–1436. [PubMed: 25526595]
2. Smith RD, Loo JA, Loo RRO, Busman M, Udseth HR. Principles and practice of electrospray ionization - mass spectrometry for large polypeptides and proteins. *Mass Spectrom Rev.* 1991; 10:359–452.
3. Wittmer D, Chen YH, Luckenbill BK, Hill HH Jr. Electrospray Ionization Ion Mobility Spectrometry. *Anal Chem.* 1994; 66:2348–2355.
4. Wu C, Siems WF, Reid Asbury G, Hill HH Jr. Electrospray Ionization High-Resolution Ion Mobility Spectrometry-Mass Spectrometry. *Anal Chem.* 1998; 70:4929–4938. [PubMed: 21644676]
5. Covey T, Douglas D. Collision cross sections for protein ions. *J Am Soc Mass Spectrom.* 1993; 4:616–623. [PubMed: 24227664]
6. Clemmer DE, Hudgins RR, Jarrold MF. Naked Protein Conformations: Cytochrome c in the Gas Phase. *J Am Chem Soc.* 1995; 117:10141–10142.
7. Shelimov KB, Clemmer DE, Hudgins RR, Jarrold MF. Protein Structure in Vacuo: Gas-phase Conformations of BPTI and Cytochrome c. *J Am Chem Soc.* 1997; 119:2240–2248.
8. Shelimov KB, Jarrold MF. Conformations, Unfolding, and Refolding of Apomyoglobin in Vacuum: An Activation Barrier for Gas-Phase Protein Folding. *J Am Chem Soc.* 1997; 119:2987–2994.
9. Valentine SJ, Counterman AE, Clemmer DE. Conformer-dependent proton-transfer reactions of ubiquitin ions. *J Am Soc Mass Spectrom.* 1997; 8:954–961.
10. Purves RW, Barnett DA, Ells B, Guevremont R. Investigation of Bovine Ubiquitin Conformers Separated By High-Field Asymmetric Waveform Ion Mobility Spectrometry: Cross Section

- Measurements Using Energy-Loss Experiments with a Triple Quadrupole Mass Spectrometer. *J Am Soc Mass Spectrom.* 2000; 11:738–745. [PubMed: 10937797]
11. Guo Y, Wang J, Javahery G, Thomson BA, Siu KWM. Ion Mobility Spectrometer with Radial Collisional Focusing. *Anal Chem.* 2005; 77:266–275. [PubMed: 15623305]
 12. Baker ES, Clowers BH, Li F, Tang K, Tolmachev AV, Prior DC, Belov ME, Smith RD. Ion Mobility Spectrometry—Mass Spectrometry Performance Using Electrodynamic Ion Funnel and Elevated Drift Gas Pressures. *J Am Soc Mass Spectrom.* 2007; 18:1176–1187. [PubMed: 17512752]
 13. Giles K, Wildgoose JL, Langridge DJ, Campuzano I. A Method For Direct Measurement of Ion Mobilities Using a Travelling Wave Ion Guide. *Int J Mass Spectrom.* 2010; 298:10–16.
 14. Mui W, Thomas DA, Downard AJ, Beauchamp JL, Seinfeld JH, Flagan RC. Ion Mobility-Mass Spectrometry with a Radial Opposed Migration Ion And Aerosol Classifier (ROMIAC). *Anal Chem.* 2013; 85:6319–6326. [PubMed: 23730869]
 15. Shrestha B, Vertes A. High-Throughput Cell and Tissue Analysis with Enhanced Molecular Coverage by Laser Ablation Electrospray Ionization Mass Spectrometry Using Ion Mobility Separation. *Anal Chem.* 2014; 86:4308–4315. [PubMed: 24684249]
 16. Li J, Taraszka JA, Counterman AE, Clemmer DE. Influence of Solvent Composition and Capillary Temperature on the Conformations of Electrosprayed Ions: Unfolding of Compact Ubiquitin Conformers from Pseudonative and Denatured Solutions. *Int J Mass Spectrom.* 1999; 185:37–47.
 17. Myung S, Badman ER, Lee YJ, Clemmer DE. Structural Transitions of Electrosprayed Ubiquitin Ions Stored in an Ion Trap Over~ 10 ms to 30 s. *J Phys Chem A.* 2002; 106:9976–9982.
 18. Jurneczko E, Kalapothakis J, Campuzano IDG, Morris M, Barran PE. Effects of Drift Gas on Collision Cross Sections of a Protein Standard in Linear Drift Tube and Traveling Wave Ion Mobility Mass Spectrometry. *Anal Chem.* 2012; 84:8524–8531. [PubMed: 22974196]
 19. Ibrahim YM, Baker ES, Danielson WF III, Norheim RV, Prior DC, Anderson GA, Belov ME, Smith RD. Development of a New Ion Mobility Time-of-Flight Mass Spectrometer. *Int J Mass Spectrom.* 2015; 377:655–662. [PubMed: 26185483]
 20. Ibrahim YM, Prior DC, Baker ES, Smith RD, Belov ME. Characterization of an Ion Mobility-Multiplexed Collision-Induced Dissociation-Tandem Time-of-Flight Mass Spectrometry Approach. *Int J Mass Spectrom.* 2010; 293:34–44. [PubMed: 20596241]
 21. Tang K, Shvartsburg AA, Lee HN, Prior DC, Buschbach MA, Li F, Tolmachev AV, Anderson GA, Smith RD. High-Sensitivity Ion Mobility Spectrometry/Mass Spectrometry Using Electrodynamic Ion Funnel Interfaces. *Anal Chem.* 2005; 77:3330–3339. [PubMed: 15889926]
 22. Ibrahim YM, Tang K, Tolmachev AV, Shvartsburg AA, Smith RD. Improving Mass Spectrometer Sensitivity Using a High-Pressure Electrodynamic Ion Funnel Interface. *J Am Soc Mass Spectrom.* 2006; 17:1299–1305. [PubMed: 16839773]
 23. Ibrahim Y, Belov ME, Tolmachev AV, Prior DC, Smith RD. Higher-Pressure Ion Funnel Trap Interface for Orthogonal Time-of-Flight Mass Spectrometry. *Anal Chem.* 2007; 79:7845–7852. [PubMed: 17850113]
 24. Clowers BH, Ibrahim YM, Prior DC, Danielson WF, Belov ME, Smith RD. Enhanced Ion Utilization Efficiency Using an Electrodynamic Ion Funnel Trap as an Injection Mechanism for Ion Mobility Spectrometry. *Anal Chem.* 2008; 80:612–623. [PubMed: 18166021]
 25. Shaffer SA, Tang K, Anderson GA, Prior DC, Udseth HR, Smith RD. A Novel Ion Funnel for Focusing Ions at Elevated Pressure Using Electrospray Ionization Mass Spectrometry. *Rapid Commun Mass Spectrom.* 1997; 11:1813–1817.
 26. Clowers BH, Belov ME, Prior DC, Danielson WF, Ibrahim YM, Smith RD. Pseudorandom Sequence Modifications for Ion Mobility Orthogonal Time-of-Flight Mass Spectrometry. *Anal Chem.* 2008; 80:2464–2473. [PubMed: 18311942]
 27. Belov ME, Clowers BH, Prior DC, Danielson WF III, Liyu AV, Petritis BO, Smith RD. Dynamically Multiplexed Ion Mobility Time-of-Flight Mass Spectrometry. *Anal Chem.* 2008; 80:5873–5883. [PubMed: 18582088]
 28. Crowell KL, Slyszyk GW, Baker ES, LaMarche BL, Monroe ME, Ibrahim YM, Payne SH, Anderson GA, Smith RD. LC-IMS-MS Feature Finder: Detecting Multidimensional Liquid Chromatography,

- Ion Mobility and Mass Spectrometry Features in Complex Datasets. *Bioinformatics*. 2013; 29:2804–2805. [PubMed: 24008421]
29. May JC, Goodwin CR, Lareau NM, Leaptrot KL, Morris CB, Kurulugama RT, Mordehai A, Klein C, Barry W, Darland E, Overney G, Imatani K, Stafford GC, Fjeldsted JC, McLean JA. Conformational Ordering of Biomolecules in the Gas Phase: Nitrogen Collision Cross Sections Measured on a Prototype High Resolution Drift Tube Ion Mobility-Mass Spectrometer. *Anal Chem*. 2014; 86:2107–2116. [PubMed: 24446877]
 30. May JC, Dodds JN, Kurulugama RT, Stafford GC, Fjeldsted JC, McLean JA. Broad-scale Resolving Power Performance of a High Precision Uniform Field Ion Mobility-Mass Spectrometer. *Analyst*. 2015; 140:6824–6833. [PubMed: 26191544]
 31. Stow SM, Causon TJ, Zheng X, Kurulugama RT, Mairinger T, May JC, Rennie EE, Baker ES, Smith RD, McLean JA, Hann S, Fjeldsted JC. An Interlaboratory Evaluation of Drift Tube Ion Mobility-Mass Spectrometry Collision Cross Section Measurements. *Anal Chem*. 2017; 89:9048–9055. [PubMed: 28763190]
 32. Kurulugama RT, Darland E, Kuhlmann F, Stafford G, Fjeldsted J. Evaluation of Drift Gas Selection in Complex Sample Analyses Using a High Performance Drift Tube Ion Mobility-QTOF Mass Spectrometer. *Analyst*. 2015; 14:6834–6844.
 33. May JC, McLean JA. A Uniform Field Ion Mobility Study of Melittin and Implications of Low-Field Mobility for Resolving Fine Cross-Sectional Detail in Peptide and Protein Experiments. *Proteomics*. 2015; 15:2862–2871. [PubMed: 25884242]
 34. Ibrahim YM, Garimella SV, Tolmachev AV, Baker ES, Smith RD. Improving Ion Mobility Measurement Sensitivity by Utilizing Helium in an Ion Funnel Trap. *Anal Chem*. 2014; 86:5295–5299. [PubMed: 24786390]
 35. Lorenzen, K., Duijn, Ev. *Current Protocols in Protein Science*. John Wiley & Sons, Inc; 2001. Native Mass Spectrometry as a Tool in Structural Biology.
 36. www.ambermd.org.
 37. Bleiholder C, Wyttenbach T, Bowers MT. A novel Projection Approximation Algorithm for the Fast and Accurate Computation of Molecular Collision Cross Sections (I). *Method. International Journal of Mass Spectrometry*. 2011; 308:1–10.
 38. Bleiholder C, Contreras S, Do TD, Bowers MT. A Novel Projection Approximation Algorithm for the Fast and Accurate Computation of Molecular Collision Cross Sections (II). Model parameterization and definition of empirical shape factors for proteins. *Int J Mass Spectrom*. 2013; 345:89–96.
 39. Anderson SE, Bleiholder C, Brocker ER, Stang PJ, Bowers MT. A Novel Projection Approximation Algorithm for the Fast and Accurate Computation of Molecular Collision Cross Sections (III): Application to Supramolecular Coordination-Driven Assemblies with Complex Shapes. *Int J Mass Spectrom*. 2012; 330:78–84.
 40. Bleiholder C, Contreras S, Bowers MT. A Novel Projection Approximation Algorithm for the Fast and Accurate Computation of Molecular Collision Cross Sections (IV). Application to Polypeptides. *Int J Mass Spectrom*. 2013; 354:275–280.
 41. Lermyte F, Łcki MK, Valkenborg D, Gambin A, Sobott F. Conformational Space and Stability of ETD Charge Reduction Products of Ubiquitin. *J Am Soc Mass Spectrom*. 2017; 28:69–76. [PubMed: 27495285]
 42. Laszlo KJ, Buckner JH, Munger EB, Bush MF. Native-Like and Denatured Cytochrome c Ions Yield Cation-to-Anion Proton Transfer Reaction Products with Similar Collision Cross-Sections. *J Am Soc Mass Spectrom*. 2017:1–10.
 43. Wyttenbach T, Bowers MT. Structural Stability from Solution to the Gas Phase: Native Solution Structure of Ubiquitin Survives Analysis in a Solvent-Free Ion Mobility–Mass Spectrometry Environment. *J Phys Chem B*. 2011; 115:12266–12275. [PubMed: 21905704]
 44. Ridgeway ME, Silveira JA, Meier JE, Park MA. Microheterogeneity within Conformational States of Ubiquitin Revealed by High Resolution Trapped Ion Mobility Spectrometry. *Analyst*. 2015; 14:6964–6972.
 45. Koeniger SL, Clemmer DE. Resolution and Structural Transitions of Elongated States of Ubiquitin. *J Am Soc Mass Spectrom*. 2007; 18:322–331. [PubMed: 17084091]

46. Zhao Q, Soyk MW, Schieffer GM, Fuhrer K, Gonin MM, Houk R, Badman ER. An Ion Trap-Ion Mobility-Time of Flight Mass Spectrometer with Three Ion Sources for Ion/Ion Reactions. *J Am Soc Mass Spectrom.* 2009; 20:1549–1561. [PubMed: 19493684]
47. Shi H, Clemmer DE. Evidence for Two New Solution States of Ubiquitin by IMS–MS Analysis. *J Phys Chem B.* 2014; 118:3498–3506. [PubMed: 24625065]
48. Bush MF, Hall Z, Giles K, Hoyes J, Robinson CV, Ruotolo BT. Collision Cross Sections of Proteins and Their Complexes: A Calibration Framework and Database for Gas-Phase Structural Biology. *Anal Chem.* 2010; 82:9557–9565. [PubMed: 20979392]
49. Allen SJ, Schwartz AM, Bush MF. Effects of Polarity on the Structures and Charge States of Native-Like Proteins and Protein Complexes in the Gas Phase. *Anal Chem.* 2013; 85:12055–12061. [PubMed: 24224685]
50. Fernandez-Lima FA, Blase RC, Russell DH. A Study of Ion-Neutral Collision Cross Section Values for Low Charge States of Peptides, Proteins, and Peptide/Protein Complexes. *International Journal for Mass Spectrometry.* 2010; 298:111–118.
51. Silveira JA, Jeon J, Gamage CM, Pai P-J, Fort KL, Russell DH. Damping Factor Links Periodic Focusing and Uniform Field Ion Mobility for Accurate Determination of Collision Cross Sections. *Anal Chem.* 2012; 84:2818–2824. [PubMed: 22404635]
52. Bleiholder C, Johnson NR, Contreras S, Wyttenbach T, Bowers MT. Molecular Structures and Ion Mobility Cross Sections: Analysis of the Effects of He and N₂ Buffer Gas. *Anal Chem.* 2015; 87:7196–7203. [PubMed: 26076363]
53. Liu FC, Kirk SR, Bleiholder C. On the structural denaturation of biological analytes in trapped ion mobility spectrometry - mass spectrometry. *Analyst.* 2016; 141:3722–3730. [PubMed: 26998732]
54. May JC, Morris CB, McLean JA. Ion Mobility Collision Cross Section Compendium. *Anal Chem.* 2017; 89:1032–1044. [PubMed: 28035808]
55. Jurnecko E, Barran PE. How useful is ion mobility mass spectrometry for structural biology? The relationship between protein crystal structures and their collision cross sections in the gas phase. *Analyst.* 2011; 136:20–28. [PubMed: 20820495]
56. Clemmer DE, Jarrold MF. Ion Mobility Measurements and their Applications to Clusters and Biomolecules. *J Mass Spectrom.* 1997; 32:577–592.
57. Dickinson ER, Jurnecko E, Pacholarz KJ, Clarke DJ, Reeves M, Ball KL, Hupp T, Campopiano D, Nikolova PV, Barran PE. Insights into the Conformations of Three Structurally Diverse Proteins: Cytochrome c, p53, and MDM2, Provided by Variable-Temperature Ion Mobility Mass Spectrometry. *Anal Chem.* 2015; 87:3231–3238. [PubMed: 25629302]
58. Valentine SJ, Clemmer DE. H/D exchange levels of shape-resolved cytochrome c conformers in the gas phase. *J Am Chem Soc.* 1997; 119:3558–3566.
59. Faull PA, Korkeila KE, Kalapothakis JM, Gray A, McCullough BJ, Barran PE. Gas-phase metalloprotein complexes interrogated by ion mobility-mass spectrometry. *Int J Mass Spectrom.* 2009; 283:140–148.
60. Zhao Q, Schieffer GM, Soyk MW, Anderson TJ, Houk RS, Badman ER. Effects of ion/ion proton transfer reactions on conformation of gas-phase cytochrome c ions. *J Am Soc Mass Spectrom.* 2010; 21:1208–1217. [PubMed: 20430642]
61. Sundarapandian S, May JC, McLean JA. Dual Source Ion Mobility-Mass Spectrometer for Direct Comparison of Electrospray Ionization and MALDI Collision Cross Section Measurements. *Anal Chem.* 2010; 82:3247–3254. [PubMed: 20329759]
62. Matz LM, Hill HH Jr, Beegle LW, Kanik I. Investigation of drift gas selectivity in high resolution ion mobility spectrometry with mass spectrometry detection. *J Am Soc Mass Spectrom.* 2002; 13:300–307. [PubMed: 11951967]
63. Schenk ER, Almeida R, Miksovska J, Ridgeway ME, Park MA, Fernandez-Lima F. Kinetic Intermediates of Holo- and Apo-Myoglobin Studied Using HDX-TIMS-MS and Molecular Dynamic Simulations. *J Am Soc Mass Spectrom.* 2015; 26:555–563. [PubMed: 25690175]
64. Benigni P, Marin R, Molano-Arevalo JC, Garabedian A, Wolff JJ, Ridgeway ME, Park MA, Fernandez-Lima F. Towards the analysis of high molecular weight proteins and protein complexes using TIMS-MS. *Int J Ion Mobil Spectrom.* 2016; 19:95–104. [PubMed: 27818614]

65. Hoaglund-Hyzer CS, Counterman AE, Clemmer DE. Anhydrous Protein Ions. *Chem Rev.* 1999; 99:3037–3080. [PubMed: 11749510]
66. Wagner ND, Kim D, Russell DH. Increasing Ubiquitin Ion Resistance to Unfolding in the Gas Phase Using Chloride Adduction: Preserving More “Native-Like” Conformations Despite Collisional Activation. *Anal Chem.* 2016; 88:5934–5940. [PubMed: 27137645]

Author Manuscript

Author Manuscript

Author Manuscript

Author Manuscript

Highlights

- Evaluation of an ion mobility-mass spectrometer for mapping protein conformations.
- Conformational landscape differences between helium and nitrogen drift gases.
- Over 260 helium and nitrogen cross section values measured for three proteins.
- Findings are compared to 470 cross section values from the literature.
- Structural preferences of previously unmeasured protein charge states are reported.

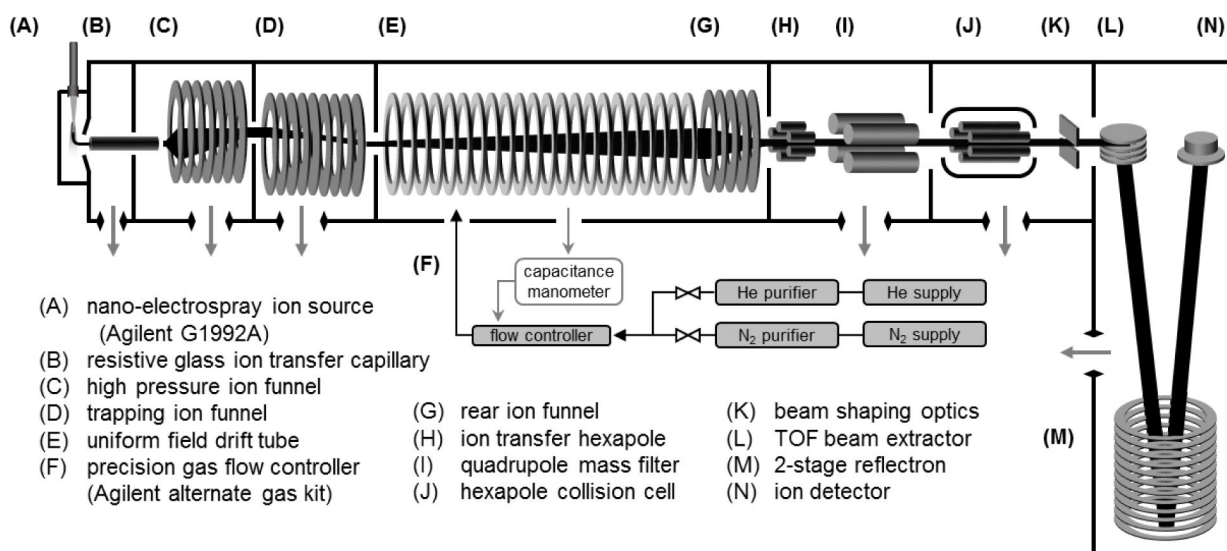


Figure 1.

A schematic of the instrumentation used in this work with main components annotated. The ion beam path is highlighted in black.

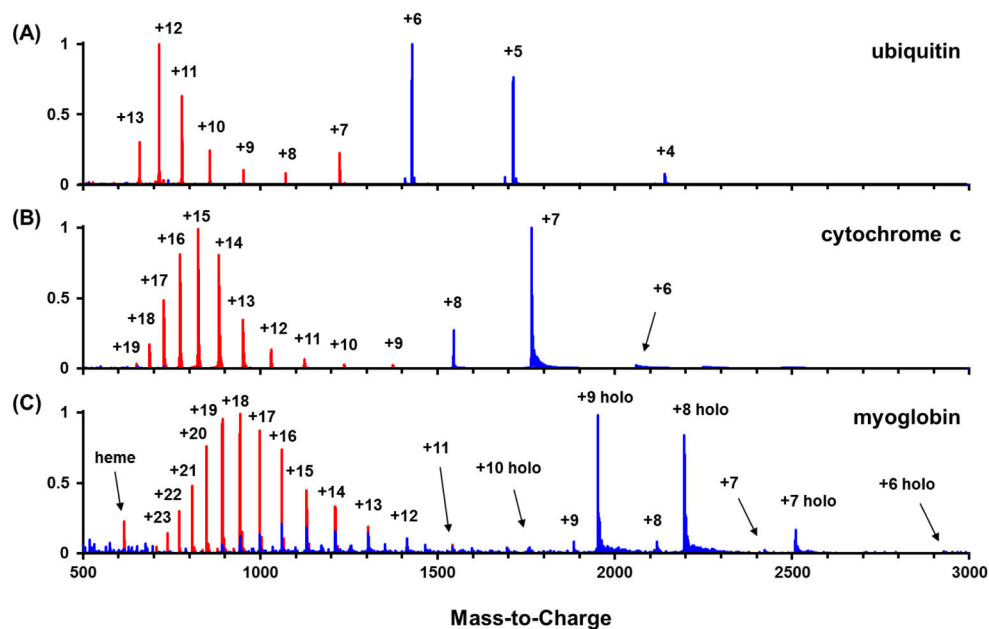


Figure 2. The mass spectra observed for (A) ubiquitin (8,566 Da), (B) cytochrome c (12,359 Da), and (C) myoglobin (apo 16,951 Da; holo 17,567 Da) electrosprayed from both acidic organic (pH ~3, red traces) and aqueous buffered (pH ~6.6, blue traces) solution conditions. For myoglobin, the charge states labeled “holo” correspond to ions which retain the heme group (616 Da). Note that each mass spectrum represents two overlaid traces, each of which is normalized to the maximum ion abundance (y-axis).

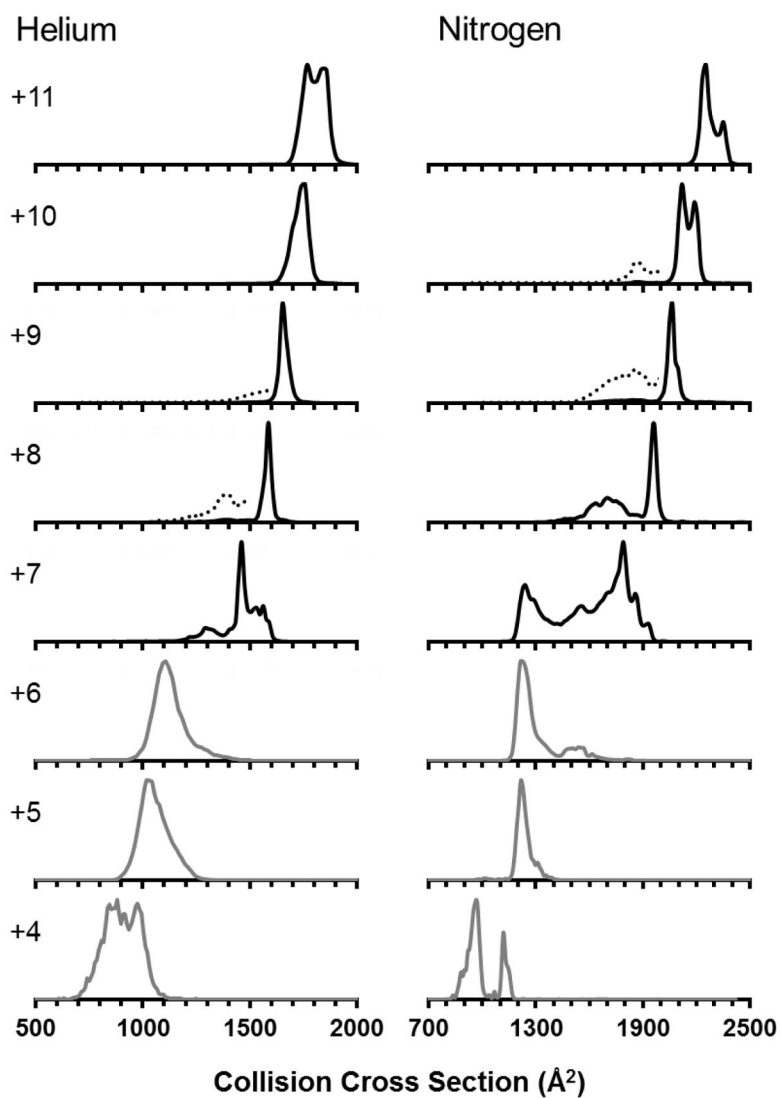
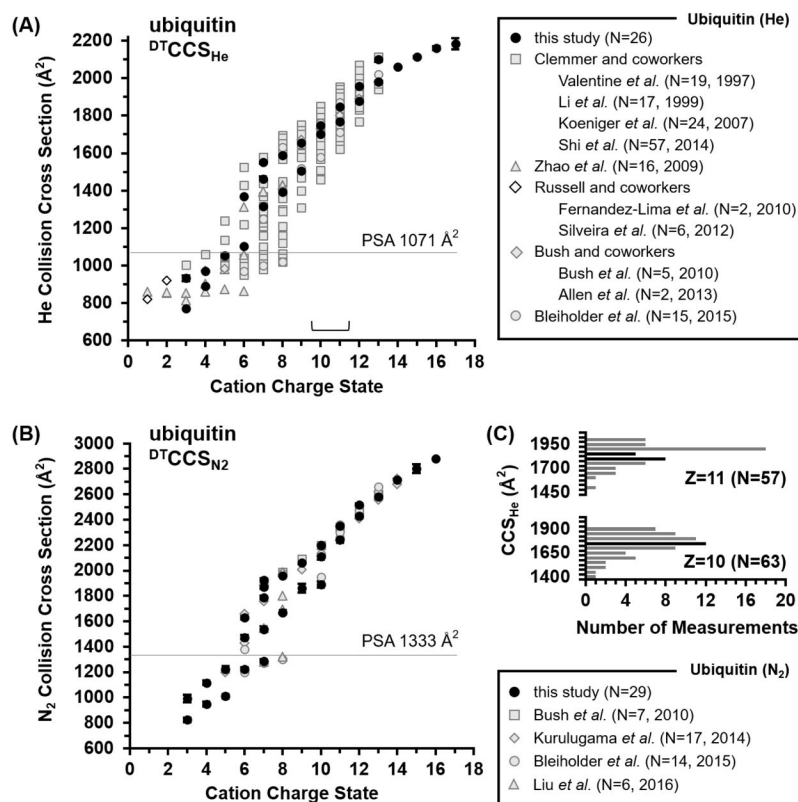


Figure 3. Extracted ion mobility spectra for selected charge states of the ubiquitin protein system measured in (A) helium and (B) nitrogen drift gas. The higher charge states (+7 to +10, dark traces) represent spectra obtained in organic solution (pH ~3), whereas the lower charge states (+4 to +6, light traces) correspond to spectra measured under aqueous buffered solution conditions (pH ~6.6). The dotted traces appearing in some of the spectra are scaled on the y-axis by a factor of 10 in relative intensity.

**Figure 4.**

Summary of the ubiquitin CCS values obtained in this work (black filled circles) with drift tube measurements published in the literature for (A) helium, and (B) nitrogen drift gases. Error bars are from replicate measurements (between 2 and 5) and are mostly covered by the size of the data points. Panel (C) contains the distributions of helium CCS literature values for the +10 and +11 charge states (bracket in panel A) with measurements from this study (dark bars). The horizontal lines in panels A and B indicate theoretical CCS values obtained from the X-ray crystal structure using the PSA method. Literature references can be found in the text.

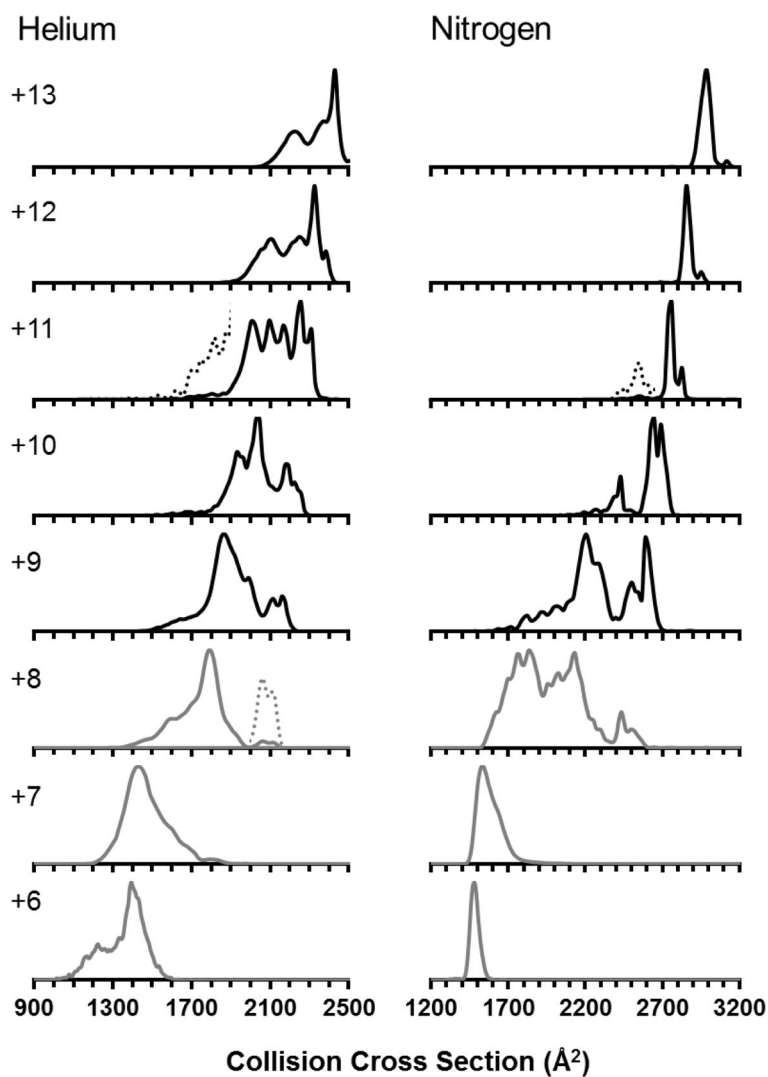


Figure 5. Ion mobility spectra for selected charge states of cytochrome c obtained in (A) helium and (B) nitrogen drift gas. The higher charge states (+9 to +13, dark traces) were obtained in acidic organic solution (pH ~3), whereas the lower charge states (+6 to +8, light traces) were measured under aqueous buffered solution conditions (pH ~6.6). Dotted traces are scaled by a factor of 10 in relative intensity.

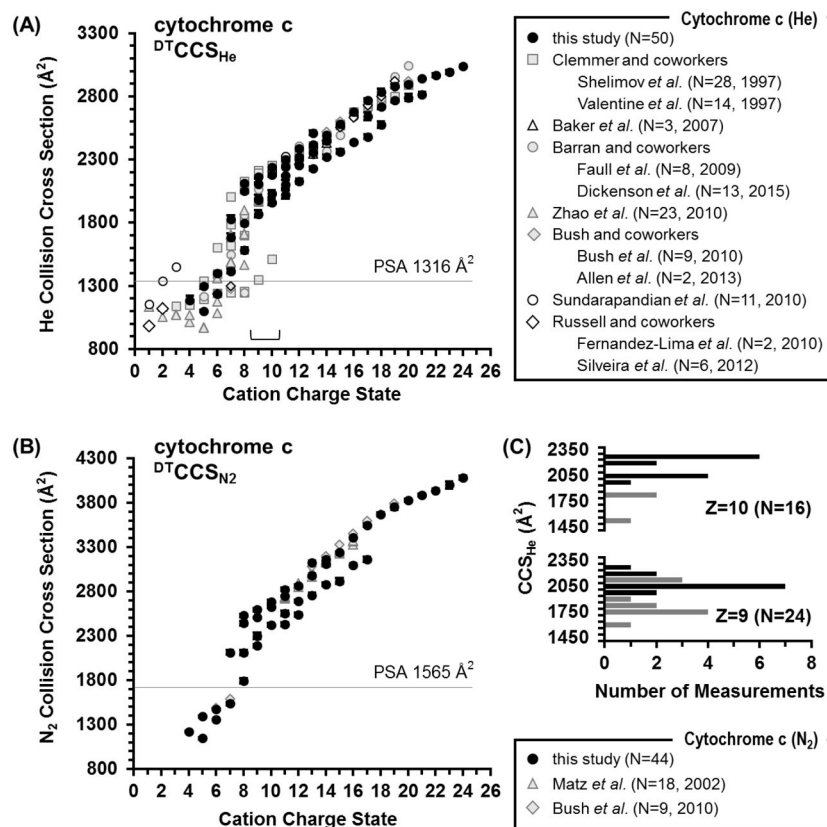


Figure 6.

A summary of cytochrome c CCS values obtained in this work (black filled circles) with drift tube results published in the literature for (A) helium, and (B) nitrogen drift gases. Error bars at mostly covered by the data points. Panel (C) contains the distributions of helium CCS literature values for the +9 and +10 charge states (bracket in panel A) where CCS bins containing values from this current study are highlighted in black. The horizontal lines in panels A and B indicate theoretical CCS values obtained from the X-ray crystal structure using the PSA method. Literature references can be found in the text.

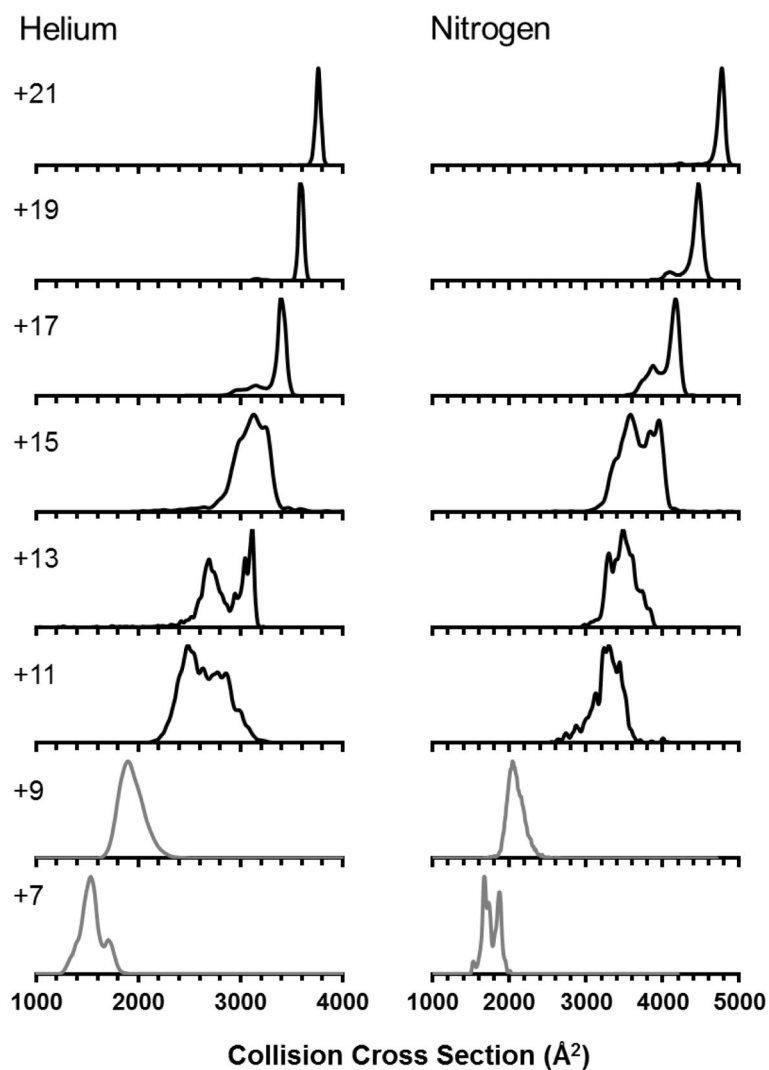
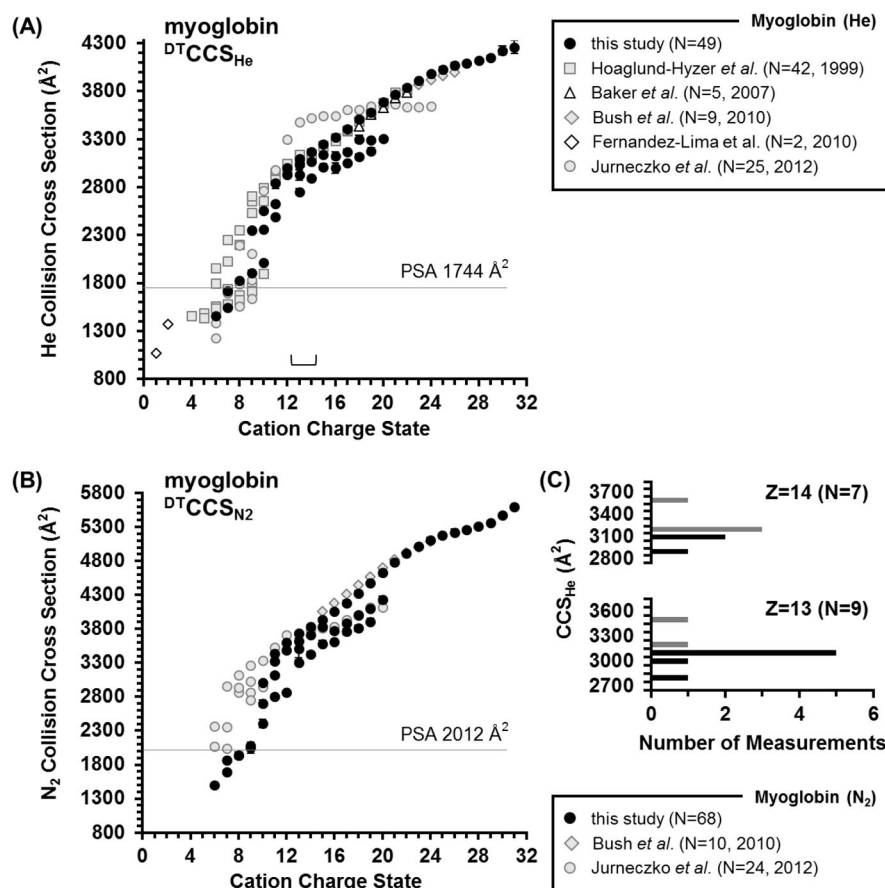


Figure 7. Ion mobility spectra for selected charge states of myoglobin measured in (A) helium and (B) nitrogen drift gases. The dark traces (+9 to +13) correspond to spectra obtained under acidic organic solution conditions (pH ~3), whereas the light traces (+6 to +8) were obtained under aqueous buffered solution conditions (pH ~6.6).

**Figure 8.**

Summary of myoglobin CCS values obtained in this work (black filled circles) with drift tube results published in the literature for (A) helium, and (B) nitrogen drift gases. In both panels, CCS values for charge states +8 and lower correspond to the holo form. Error bars are mostly covered by the data points. Panel (C) contains the distributions of helium CCS literature values for the +13 and +14 charge states (bracket in panel A) where CCS bins containing values from this current study are highlighted in black. The horizontal lines in panels A and B indicate theoretical CCS values obtained from the X-ray crystal structure using the PSA method. Literature references can be found in the text.